IEEE Access
Multidisciplinary | Rapid Review | Open Access Journal

Received December 16, 2020, accepted December 21, 2020, date of publication December 29, 2020,
date of current version January 28, 2021.

Digital Object Identifier 10.1109/ACCESS.2020.3048029

Design and Sensitivity Analysis of Dynamic Wireless Chargers for Efficient Energy Transfer

S. ABBAS MOOSAVI[1], S. SAEIDALLAH MORTAZAVI[1], ALIREZA NAMADMALAN[2], ATIF IQBAL[3], (Senior Member, IEEE), AND MOHAMMED AL-HITMI[3], (Member, IEEE)

[1]Department of Engineering, Shahid Chamran University of Ahvaz, Ahvaz 6135743136, Iran
[2]Department of Electrical and Computer Engineering, Jundi-Shapur University of Technology, Dezful 64617-96736, Iran
[3]Department of Electrical Engineering, Qatar University, Doha, Qatar

Corresponding author: Mohammed Al-Hitmi (m.a.alhitmi@qu.edu.qa)

This publication was made possible by Qatar University Collaborative Research grant # [QUCG-CENG-19/20-5] from the Qatar University. The statements made herein are solely the responsibility of the authors. The APC is funded by the Qatar National Library, Doha, Qatar.

ABSTRACT Tunable Self-Oscillating Switching (TSOS) methods are a robust solution for tuning of Inductive Power Transfer (IPT) systems. However, they require deep analysis to be an appropriate choice for Dynamic Wireless Charging (DWC) systems. In this paper, the optimal operation point of TSOS in the maximum power transfer, efficiency, and Zero Voltage Switching (ZVS) realization perspectives are determined based on sensitivity analysis for DWC of Electric Vehicles (EVs). In the sensitivity analysis, all the possible states of the coupling factor and state of charge (SOC) are considered as system variables. Moreover, a new phasor modeling for constant voltage (battery) loads is proposed. The performance of this model is quite different from the conventional static model for the loads. Moreover, to limit the current of the charger under light couplings, a simple hysteresis controller is employed. A setpoint is proposed based on the sensitivity analysis method to transfer maximum energy in misaligned conditions. The proposed setpoint increases transferred energy and energy efficiency while limits the current of the charger. To analyze this method, simulation is done in the Simulink/MATLAB, and to verify the results, a laboratory prototype is implemented.

INDEX TERMS Electric vehicles, inductive charging, resonant inverters, tunable circuits and devices, zero voltage switching.

I. INTRODUCTION

The wireless power transfer (WPT), which enables electric power transferring from the transmitter to the receiver over a large air gap, is developing rapidly [1]–[5]. In WPT, the power transfer coupler can be completely sealed, because no direct connection is needed. This provides protection against intrusion, dust, water, snow, and chemicals and makes it suitable for power supply applications in the harsh environment [6], [7]. There are many applications for WPT, including cell phones, medical implants, and electric vehicles (EVs) charging [4], [8]. In addition to electric shock risks reduction and ease of use for the disabled or the elderly, WPT makes it possible to charge EVs on the go, which is called dynamic wireless charging (DWC) [9]–[11]. With DWC realization, the range anxiety problem could be eliminated [12], [13].

The associate editor coordinating the review of this manuscript and approving it for publication was Sanjeevikumar Padmanaban.

Inductive power transfer (IPT) is the most popular method of WPT [14]. IPT works like a transformer with a large air gap. Hence, a large magnetization current will pass through the track coil. Moreover, a compensation network is used to compensate for this reactive current. The most common compensation network is series-series (SS), which has some advantages including simplicity, high power transfer capability, high misalignment tolerance, and the fact that the primary capacitor is independent of secondary side parameters [8], [15].

To modeling the IPT system, usually, a constant resistor is used as the equivalent of battery load [8], [16], [17]. Changes in the state of charge (SOC) of battery, frequency, and/or coupling factor lead to changes in equivalent resistance of the load. Therefore, using a constant resistor for the battery load modeling, especially in DWC, is not accurate.

To control the IPT system, there are some switching control methods including constant frequency and variable frequency

control like power-frequency, phase-shift and sliding mode control, that may use phase-locked loop (PLL) [18], [19] and Self-Oscillating Switching (SOS) techniques [20]–[23]. Despite the simplicity of control, because of the dynamics of the system in DWC, the constant frequency method does not operate in optimal condition. Most of variable frequency control methods depend on the wireless data transfer between the charger and the load. To eliminate the wireless data transfer equipment in the vehicles, a universal charger should work with high efficiency without secondary side data. Self-tuning capability is suitable for WPT in which system characteristics change due to load movement and misalignment, especially in DWC. Hence, the charger must adapt to new conditions or be robust against changes. When system characteristics are changed, the switching frequency of the SOS-based system is changed subsequently. The new operating point of the system may be not a proper point in efficiency and power transfer perspective. By adding a phase shifter to SOS and creating a tunable SOS (TSOS), the operating point and the switching frequency of the system can be tuned in a proper point [21], [22]. The TSOS is fast enough to track a proper operating point, which leads to realizing zero voltage switching (ZVS) in all operating conditions. Also, it is robust enough and those variations do not affect its proper function. Because of continuous variation in the DWC and probable bifurcation phenomenon, and complicated phase and impedance transfer functions of IPT, a frequency tuning loop based on PLL might affect the stability and dynamics of the system.

To encourage people to use EVs and more satisfaction with using other electrical devices, fast charging should be developed. Hence, the maximum power transfer in a reasonable efficiency is necessary for developing wireless charging. Therefore, this paper investigates TSOS-based IPT to find the optimal operation point in a maximum power transfer perspective. In previous papers, changing the equivalent resistance of load in DWC is not considered precisely. In this paper, an accurate model for equivalent resistance of the load is presented to cover the DWC condition. In the case of DWC or severe misalignment, there is a possibility of a very low coupling condition, which leads to an excessive increase in system currents. To overcome this trouble, a simple hysteresis current control is used to limit and control the input current and power. A sensitivity analysis is done to determine the setpoint of hysteresis current control to achieve maximum energy efficiency in the maximum misalignment conditions. In brief, this paper presents a simple and robust tuning method of the IPT system for the DWC application.

This paper is structured as follows: Section II describes the fundamentals and modeling of the inductive charging system and proposes a new model of constant voltage loads. Section III describes TSOS to tune the system. In section IV, a sensitivity analysis of the system's variables is represented. Section V describes a current controller based on the optimum point that is determined in section IV. Also in this section, the setpoints of the current controller are designed

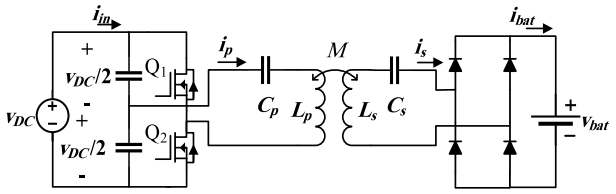

FIGURE 1. Schematic of the IPT system based on SS compensating network.

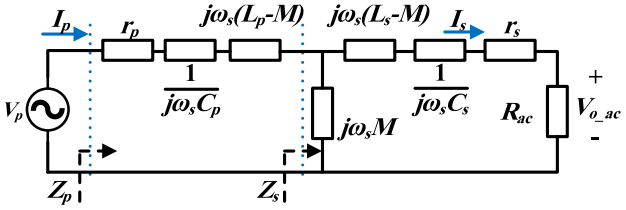

FIGURE 2. First harmonic equivalent circuit considering parasitic coil resistances.

to transfer maximum energy in misaligned conditions. The experimental results are represented in section VI, and section VII concludes the paper.

II. IPT SYSTEM MODELING AND FORMULATIONS

Fig. 1 represents the IPT system with SS compensation network. This circuit includes a DC voltage source, voltage source inverter, coupled windings to transfer power wirelessly, compensation capacitors, a rectifier, and a chargeable Li-Ion battery pack.

In Fig. 1, L_p and L_s are primary and secondary coil inductances, respectively. V_{bat}, i_{bat}, and i_{in} are battery voltage, battery current, and input DC current, respectively. Track and pickup coils are compensated by capacitors C_p and C_s which are in series with L_p and L_s, respectively. The relationship between primary and secondary capacitors, inductors, and natural angular frequency, ω_n, of the system is as (1):

$$\omega_n = 1/\sqrt{L_p C_p} = 1/\sqrt{L_s C_s} \tag{1}$$

Mutual inductance M between track and pickup coils and coupling factor k are related according to (2):

$$k = M/\sqrt{L_p L_s} \tag{2}$$

Because of the nonlinearity and dynamic characteristic of the battery, it is very complicated to analytically indicate the operation point of the system. To show this complexity, Fig. 2 is considered as the first harmonic equivalent circuit. Note that the load is a battery pack and variation of its voltage is not significant.

Capital letters are used to name phasor variables and lowercase letters are used to name the time domain variables. ω_s is switching angular frequency. V_p is the amplitude of the fundamental frequency of a square wave voltage, I_p and I_s are amplitudes of track and pickup coils currents, R_{ac} is the equivalent resistance of load reflected on the ac side of the

rectifier, and r_p and r_s are parasitic resistances of primary and secondary coils, respectively.

$$v_p(t) = V_p \sin(\omega_s t) + V_{p3} \sin(3\omega_s t) + \dots \quad (3)$$

$$V_p = 2\,V_{DC}/\pi \quad (4)$$

$$I_p = \frac{V_p}{|Z_p|}\angle\varphi. \quad (5)$$

$$Z_p = r_p + j(\omega_s L_p - \frac{1}{\omega_s C_p}) + (\omega_s M)^2 \Big/ \left(R_{ac} + r_s + j(\omega_s L_s - \frac{1}{\omega_s C_s})\right) \quad (6)$$

φ is the angle between V_p and I_p. The V_p and amplitude of input voltage of rectifier V_{o_ac} are related by (7).

$$\left|\frac{V_p}{V_{o\_ac}}\right| = \left|\frac{1}{j\omega_s M R_{ac}}\left[\begin{array}{l}\left(\begin{array}{l}\omega_s^2 M^2 + r_p(r_s + R_{ac}) \\ -(\omega_s L_p - \frac{1}{\omega_s C_p})(\omega_s L_s - \frac{1}{\omega_s C_s})\end{array}\right) \\ +j\left(\begin{array}{l}(\omega_s L_p - \frac{1}{\omega_s C_p})(r_s + R_{ac}) \\ +r_p(\omega_s L_s - \frac{1}{\omega_s C_s})\end{array}\right)\end{array}\right]\right| \quad (7)$$

Considering half-bridge topology for the inverter and a full-wave rectifier, voltage gain G_v can rewrite as (8):

$$G_v = \left|V_p / V_{o\_ac}\right| = \left|(V_{DC}/2)/V_{bat}\right| \quad (8)$$

From (7) and solving (9), R_{ac} is obtained as (10).

$$\begin{aligned} &aR_{ac}^2 + bR_{ac} + c = 0 \\ &a = r_p^2 + X_p^2\alpha^2 - X_M^2 G_v^2 \\ &b = 2r_s X_p^2\alpha^2 + 2r_s r_p^2 \\ &c = \alpha^2(r_p^2 X_s^2 + r_s^2 X_p^2 - 2X_M^2 X_p X_s + X_p^2 X_s^2\alpha^2) \\ &\quad + r_p^2 r_s^2 + X_M^4 \end{aligned} \quad (9)$$

$$R_{ac} = \frac{\left[\begin{array}{l}-r_s(X_p^2\alpha^2 + r_p^2) \\ -\sqrt{\begin{array}{l}(X_M^2 - X_p X_s\alpha^2)^2 \times (G_v^2 X_M^2 - X_p^2\alpha^2 - r_p^2) \\ +G_v^2 X_M^2 \times (r_p^2 X_s^2\alpha^2 + r_s^2 X_p^2\alpha^2 + r_p^2 r_s^2) \\ -r_p^2 X_s^2\alpha^2(1 + X_p^2\alpha^2)\end{array}}\end{array}\right]}{r_p^2 + X_p^2\alpha^2 - G_v^2 X_M^2} \quad (10)$$

that

$$X_M = \omega_s M, X_p = \omega_s L_p,\ X_s = \omega_s L_s,\ \alpha = 1 - \left(\omega_n/\omega_s\right)^2 \quad (11)$$

R_{ac} is a nonlinear function of ω_s, M, and G_v. According to (10), it is possible to calculate φ, P_{out}, and η.

$$P_{out(ac)} = \left|V_{o\_ac}\right|^2 \Big/ 2R_{ac} \quad (12)$$

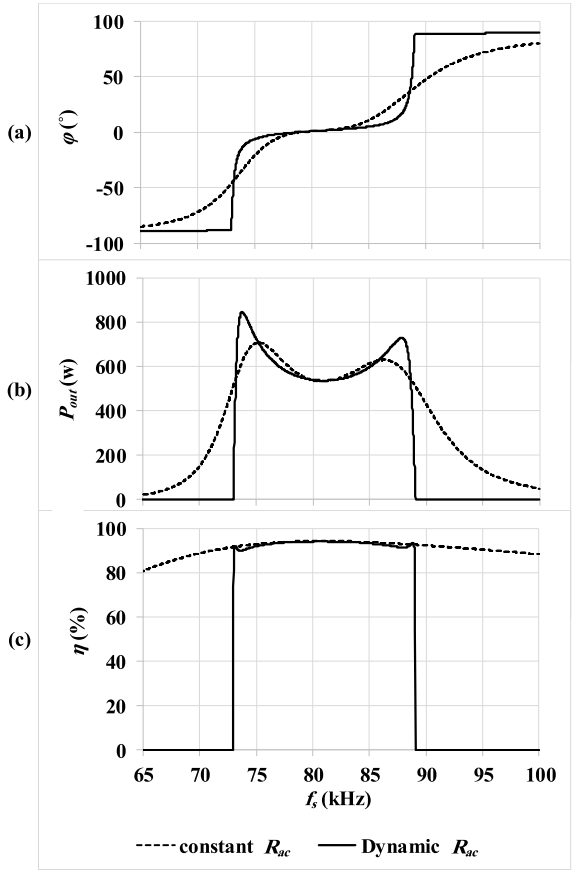

FIGURE 3. Characteristics of the IPT system with two types of R_{ac} (a) phase angle, (b) output power, and (c) efficiency.

The output power of the AC part of the circuit is obtained as (12). According to (5), (6), (10), (11), and (12), efficiency η can be calculated as (13).

$$\eta = P_{out}/P_{in} \times 100 = R_{ac} \Big/ \left(R_{ac} + r_s + r_p\frac{(R_{ac} + r_s)^2 + X_s^2\alpha^2}{X_M^2}\right) \quad (13)$$

R_{ac} depends on f_s, M, and G_v. This is an accurate model for load in DWC that has not been considered in previous papers. Previous researches in IPT systems have utilized a nominal static ohmic load for modeling of battery loads [16], [17]. Fig.3 represents the phase angle, output power, and efficiency of the IPT system with the constant resistor and new dynamic resistor as the equivalent of the battery load. The coupling factor of the system is 0.2. Other parameters of simulations are as Table 1.

Changing in the coupling factor and frequency leads to a change in R_{ac}. Therefore, the frequency response of the system in the DWC, considering the fact that R_{ac} is constant, is not accurate and the results will be different from the real condition.

According to Fig. 3 (b) and (c), power transfer is realized in a limited bandwidth, and out of this band, R_{ac} is infinite and transferring power to the load is impossible. Fig. 3 (a)

TABLE 1. Parameters of the simulated system.

PARAMETER	VALUE
V_{DC}	210 V
The nominal voltage of the battery	120 V
r_p	0.3 Ω
r_s	0.7 Ω
C_p	25 nF
C_s	16.84 nF
L_p	159 mH
L_s	236 mH
SOC	20~90%
k	0~0.2
Natural Frequency	79.828 kHz
Switching Frequency	80 kHz < f_s < 90 kHz

shows that in the outside of the power transfer band, φ tends to 90° or −90°. It should be noted that the peak of the power transfer curve is greater in dynamic R_{ac} mode than in constant R_{ac} mode.

Note that in the calculation of efficiency, the inverter and rectifier losses are neglected. Therefore, efficiency in experimental results is lower than in the theoretical results.

V_{o_ac} depends on the SOC of the battery pack. In Li-Ion batteries while SOC remains in the range of 20 to 90 percent, the voltage variation will be negligible. Hence it seems that voltage gain is approximately constant.

Because of the nonlinearity of (10), it is very complicated to analytically indicate the maximum power transfer and efficiency. To analyze the power transfer and efficiency, the procedure is simulated in MATLAB software. To indicate the maximum power transfer and efficient performance, a sensitivity analysis is used. In this method, the variables are changed in all possible ranges. Then, efficiency and output power are calculated (in MATLAB) or measured (in the laboratory) in all cases.

III. CONRTOL OF SYSTEM

TSOS is a proper method for switching control in the IPT system since its resonant frequency tracking is fast and it is robust to variation of coupling factor and load [20]–[22]. The TSOS block diagram is shown in Fig. 4.

In the presented method, the secondary side data are not used to increase the reliability and reduce the equipment cost of the vehicle. The tuning loop has one input signal, *Sig*, to start/stop the self-oscillation. By turning on *Sig*, the inverter starts switching; hence, a step voltage is applied to the series-series network. At the first zero crossing of the primary current, Q_1 is turned off and Q_2 is turned on. Similarly, the next transition repeats at the next zero crossings; hence the system operates under self-oscillation condition.

The TSOS works in an optimal operating point by applying a proper phase φ, which is the angle between V_p and I_p. φ

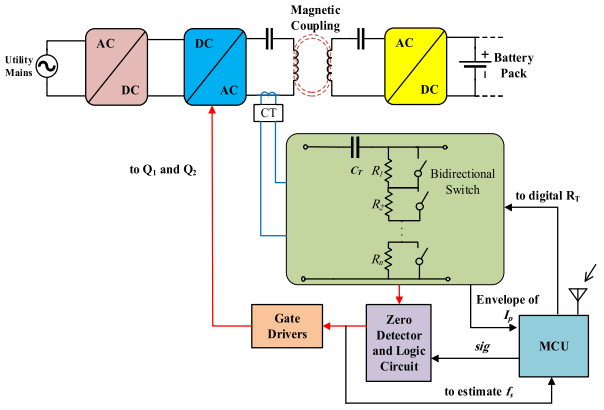

FIGURE 4. Resonant inverter tuning system based on TSOS method.

can be obtained by measuring and analyzing I_p. Then, it is applied to the system by a phase shifter. Consequently, ZVS is realized in lagging operating conditions.

According to [22], to achieve a specific φ, R_T can be tuned as (14)

$$\varphi = \angle Z_p(j\omega_s) = \tan^{-1}\left(1/(\omega_s R_T C_T)\right) \Rightarrow R_T = 1/(\omega_s C_T \tan\varphi) \quad (14)$$

Parameters of R_T and C_T are the tuning resistor and capacitor, respectively.

The operating point can be achieved considering that the phase plot of the resonant circuit is equal to the phase shifter phase displacement. If the goal is fast charging, i.e. high energy transferring is required, $R_{ac} < M\omega_n$ and bifurcation phenomenon occurs. Then, there will be three zero voltage and zero current switching (ZVZCS) points and three possible answers, while the TSOS tracks the frequencies higher than the third ZVZCS point and still ZVS will be realized [23]. However, typically the system parameters are designed optimum to prevent the bifurcation phenomenon [24].

IV. SENSITIVITY ANALYSIS OF THE SYSTEM'S VARIABLES

The main variables of the IPT system are the coupling factor and the SOC of the battery. If the track coil is very long [25] or unequal double D (UDD) [26] coil is used, the coupling factor will be constant in a range of operation. This paper uses UDD coils that explain in section V. It is more possible to have a misalignment in DWC and k will change while EV is charging and the maximum of k, k_{max}, may not occur even in static charging. Another variable in the IPT system is SOC or battery voltage. The possible range of variations for k and SOC and other parameters of the simulated DWC system are tabulated in Table 1.

Fig. 5 represents φ vs. f_s in $k = 0.2$. According to this, when V_{bat} is lower than 123V (G_v is greater than 0.853) the bifurcation occurs. The ratio of V_{DC} and the nominal voltage of the battery is chosen to prevent bifurcation at $k_{max} = 0.2$.

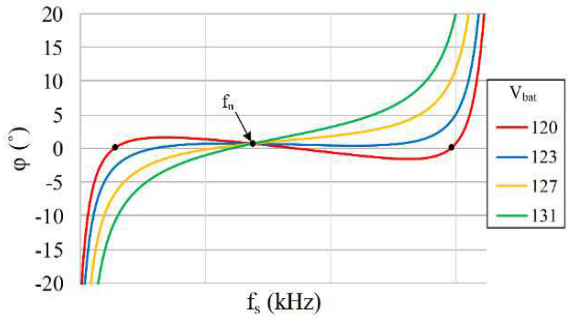

FIGURE 5. The phase of total impedance vs. switching frequency in different voltage gain and $k = 0.2$.

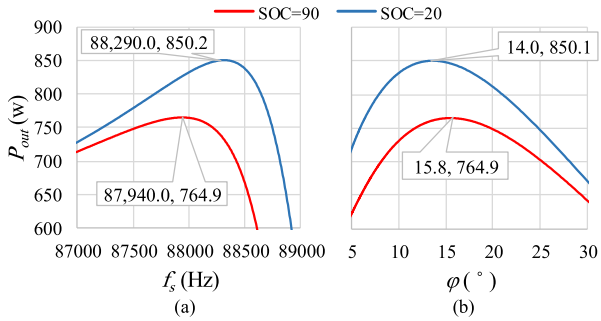

FIGURE 6. The output power vs. (a) f_s and (b) φ in two different SOC and $k = 0.2$.

A. VARIATION OF SOC

Variation of SOC in the range of 20-90% leads to a variation of V_{bat} and G_v in the range of 127-131V and 0.8268-0.8015, respectively. The variation of G_v is about 3%. Therefore, the main characteristics of the system, like the power transfer curve, do not change significantly. To investigate this, according to (12), the output power of the system is presented in Fig. 6.

According to Fig. 6 (a), changing in SOC in a possible range leads to a small change in output power curves. P_{max} changes because of SOC variation and it displaces versus f_s. In Fig. 6 (b) P_{out} is shown versus φ. In a constant coupling factor, the peak of the power transfer versus φ, P_{max}, does not displace by a change in SOC. Therefore, P_{max} is realized at a specific phase angle.

B. VARIATION OF THE COUPLING FACTOR

Change in the coupling factor leads to change in reflected resistance to primary and therefore, power transfer and I_p curves will change. In SS compensated IPT system, according to (5), (6), and (10), a decrease in M leads to a reduction in R_{ac} and Z_p, and therefore, current and power transfer increase.

Fig. 7 (a) represents P_{out} with respect to the f_s and φ in various k. According to Fig. 7 (a), by changing k, P_{max} is obtained at various frequencies. Fig. 7 (b) shows that in different k, P_{max} occurs at a specific range of φ. Therefore, the application of constant frequency methods for DWC is

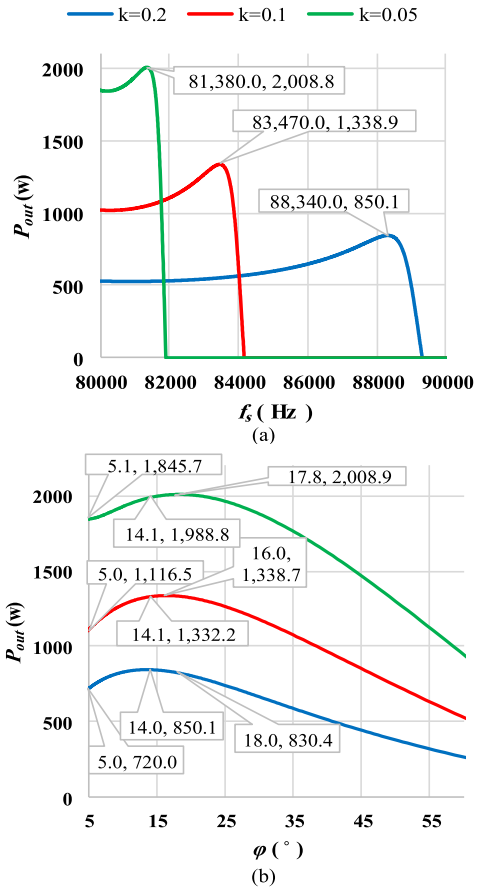

FIGURE 7. The output power of IPT with respect to (a) f_s and (b) φ in various k and SOC = 20.

complicated, because the maximum power transfer occurred in different frequencies.

C. MAXIMUM POWER TRANSFER POINT

Considering Fig. 7, the maximum power transfer takes place in the range of 14° to 18°. To show the maximum tolerance of power transfer in this range, power deviation (PD) is defined as (15):

$$PD = (P_{\max} - P_{\min}) \big/ P_{\max} \times 100 \tag{15}$$

PD shows the robustness of P_{out} against phase changes. P_{min} and P_{max} are the minimum and maximum power transfer in each condition, respectively. In this range of φ, PD in the worst case is 2.3% for $k = 0.2$ and SOC = 20%.

$$\left.\begin{aligned} \varphi = 14.0 \Rightarrow P_{\max} = 850.1 \\ \varphi = 18.0 \Rightarrow P_{\min} = 830.4 \end{aligned}\right\} \Rightarrow PD = \frac{850.1 - 830.4}{850.1} \times 100 = 2.3\% \tag{16}$$

In other cases, PD is less than 2.3%. Therefore, in this range of φ, the maximum power transfer is robust to phase changes. Variation in the coupling factor changes P_{max}, but the displacement of P_{max} against φ is insignificant.

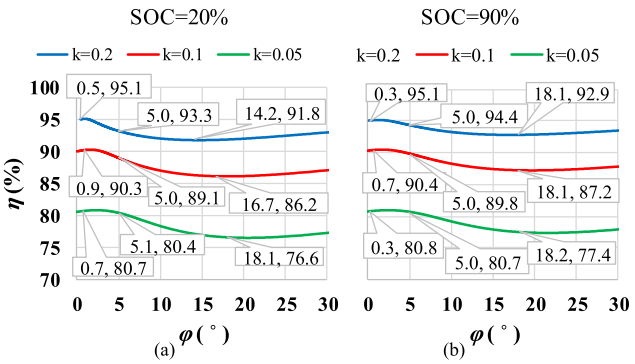

FIGURE 8. The efficiency of IPT with respect to φ in various coupling factor (a) SOC=20%, (b) SOC=90%.

It should be noted that big changes in G_v displace the peak of the power transfer curve. In other words, when the amount of changes in G_v is large, the maximum power transfer occurs in a different φ. This problem could be solved by standardization of the nominal voltage of the battery.

Transmission of the maximum feasible power to the batteries in a defined time interval (fast charge) is an important principle to develop WPT for EVs charging. The control system is simplified using the specific φ for TSOS to maximize power transfer. Note that efficiency must not decrease significantly.

In Fig. 8, efficiency curves in all cases are presented. According to these figures, efficiency is in an acceptable range. In all cases, the maximum efficiency is achieved in ZVZCS point, $\varphi = 0$. Efficiency is reduced because of an increase in φ. The maximum achievable efficiency is realized in $\varphi = 5°$ to guarantee ZVS realization. The reduction in efficiency in the range of 5° to 18° is 3.8% for the worst case that is SOC = 20% and $k = 0.05$. Operating in $\varphi = 5°$ (the maximum efficiency) leads to more than 15% reduction in the power transfer for $k = 0.2$ and SOC = 20%, as presented in Fig. 7 (b).

Therefore, setting the phase angle to the range of 14° to 18° leads to the maximum power transfer to the load as well as acceptable efficiency, which is a good compromise between efficiency and power transfer. In the next section, using this range of φ, a simple current controller is devised to limit the current and power under low coupling transitions. Using sensitivity analysis, the setpoints of the current controller are determined to maximize the transferred energy under misalignment conditions.

V. CURRENT AND POWER CONTROL

According to the previous section, by tuning φ the maximum power transfer to the load could be achieved. As mentioned before, a reduction in the coupling factor leads to an increase in the current and power transfer. Because of misalignment and when EV reaches or leaves the charger coils in DWC, the coupling factor decreases inevitably. Dimensions of UDD coils used in simulations are as Fig. 9.

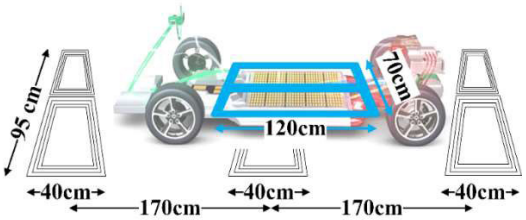

FIGURE 9. The layout of the simulated case study and dimensions of the track and pickup coils.

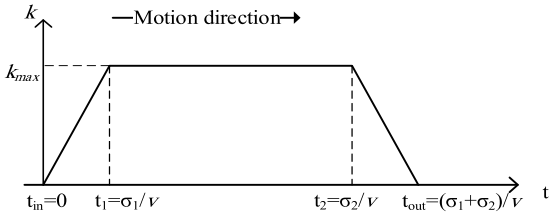

FIGURE 10. Approximated profile of k.

As EV moves toward the track coil, coupling factor changes as (17) and Fig. 10, where σ_1 and σ_2 are 40cm and 120 cm, respectively.

$$k = \begin{cases} \left(\dfrac{k_{\max} v}{\sigma_1}\right) t & t \le \dfrac{\sigma_1}{v} \\ k_{\max} & \dfrac{\sigma_1}{v} \le t \le \dfrac{\sigma_2}{v} \\ -\dfrac{k_{\max} v}{\sigma_1} \times \left(t - \left(\sigma_1 + \dfrac{\sigma_2}{v}\right)\right) & \dfrac{\sigma_2}{v} \le t \le \dfrac{\sigma_1 + \sigma_2}{v} \end{cases} \tag{17}$$

A significant reduction in the coupling factor results in a severe increase in the current and may damage the equipment. To limit the current, a simple hysteresis controller can be used [27], [28]. This controller output is fully on or fully off and applies the full power to the process or turns the process off completely. This method limits the power and current in an admissible range, while efficiency does not decrease significantly. To limit the current, the setpoint of the current controller is defined as (18):

$$I_{sp} = I_{p(\max)} / I_n \tag{18}$$

that I_{sp} and $I_{p(max)}$ are the setpoints of the current controller in per-unit and ampere, respectively. I_n is the nominal current of charger that is assumed in the maximum coupling condition and $\alpha = 0$ ($\omega_s = \omega_n$). I_n is calculated as (19):

$$I_n = V_p / |Z_p| \Big|_{\substack{\alpha=0 \\ k=k_{\max}}} = \frac{2}{\pi} V_{DC} \Big/ \left(r_p + X_M^2 / (R_{ac\,n} + r_s)\right) \tag{19}$$

that R_{acn} is as (20):

$$R_{ac}\,|_{\alpha=0} = R_{ac\,n} = \frac{-r_s r_p^2 - \sqrt{X_M^6 G_v^2 - X_M^4 r_p^2 + X_M^2 G_v^2 r_p^2 r_s^2}}{r_p^2 - X_M^2 G_v^2}$$

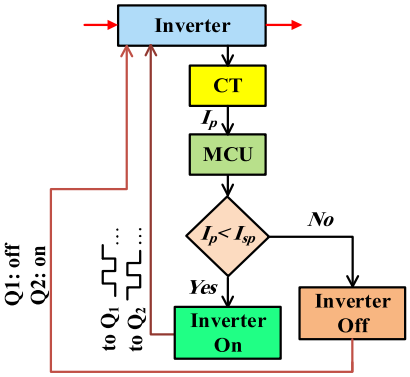

FIGURE 11. Flowchart of the current control.

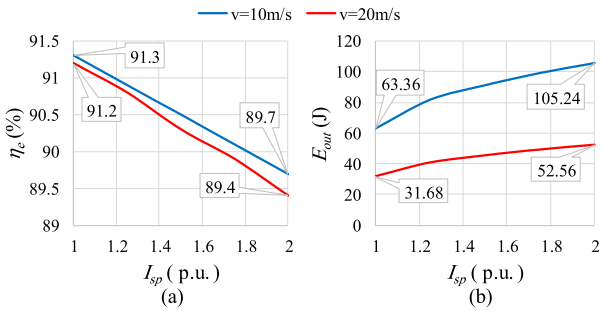

FIGURE 12. (a) Energy efficiency and (b) output energy with respect to the setpoint of the current controller at different speeds and $k_{max} = 0.2$.

(20)

Considering parameters of the system I_n and R_{acn} could be calculated. It is worth noting that the optimum operating range of the system for achieving the maximum power transfer is $14° < \varphi < 18°$. Therefore, in this range, I_p is bigger compared to $\varphi = 0$, i.e. $\omega_s = \omega_n$, condition.

The current control flowchart is presented in Fig. 11. The simulations are carried out at two different speeds: 10 and 20 m/s. It is assumed that the vehicle reaches the charger and crosses over it at a constant speed. Thus, k is varied according to (17). When k is lower than its nominal value, the current exceeds the $I_{p(min)}$, that is the minimum current of the charger that enables the maximum power transfer. According to parameters of Table 1, $I_{p(min)}$ is about 12A.

In this paper, the overcurrent tolerance is investigated to determine the proper setpoint of the current controller. The setpoint of the current controller is increased from $I_{p(min)}$ to $2I_{p(min)}$ to calculate the energy efficiency and transferred energy to the battery, as Fig. 12. These figures are obtained by simulations and (21)-(25):

$$P_{out}(M, \varphi_0) = v_{bat} \times i_{bat} \tag{21}$$

$$E_{out} = \int_0^{t_{out}} P_{out}.dt \tag{22}$$

$$P_{in}(M, \varphi_0) = V_{DC} \times i_{in} \tag{23}$$

$$E_{in} = \int_0^{t_{out}} P_{in}.dt \tag{24}$$

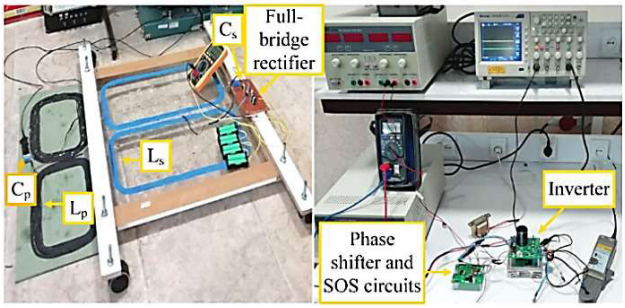

FIGURE 13. Experimental setup of the IPT system.

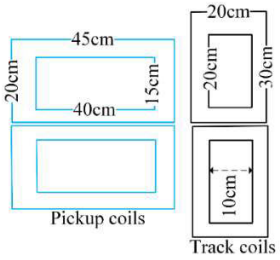

FIGURE 14. Dimensions of pickup and track coils.

$$\eta_e = E_{out}/E_{in} \times 100 \tag{25}$$

that E_{out}, E_{in}, η_e are output energy, input energy, and energy efficiency of the system, respectively. φ_0 is the optimum phase angle determined in section IV and in the following simulations is considered 15°. The integration period is 0 to t_{out} that depends on the speed of EV and coils dimensions.

In Fig. 12 (a), η_e versus I_{sp} in two speeds and $k_{max} = 0.2$ is presented. According to Fig. 12 (a), increasing I_{sp} leads to a decrease in η_e. Losses increase because of the increase in current and as a result, efficiency decreases.

Fig. 12 (a) shows that a higher speed of vehicle leads to lower efficiency. This is because of the dynamics of the IPT system. A higher speed of vehicle leaves less time for the system to settle and reach the maximum efficiency.

In Fig. 12 (b), E_{out} versus I_{sp} is presented. The higher speed of EV leaves it less time to receive energy. Increasing I_{sp} leads to more energy transfer while k is lower than k_{max}.

In Fig. 12 increasing I_{sp} from 1 to 2 p.u. leads to a 66% increase in E_{out}, while η_e decreases lower than 1.8%. Therefore, E_{out} is a more important factor to indicate I_{sp}. The rate of increase in E_{out} versus I_{sp} is linear approximately.

Choosing higher I_{sp} leads to more energy transfer and slightly lower efficiency. Although, more I_{sp} results in higher current stress and, therefore, more expensive equipment is required.

VI. EXPERIMENTAL RESULTS

To verify the simulation results, a laboratory prototype is implemented as Fig. 13 and Table 2. The primary and secondary coils are wound with 5 and 3 insulated strands of AWG 24, respectively. For $n_1 = 12$ and $n_2 = 10$ turns

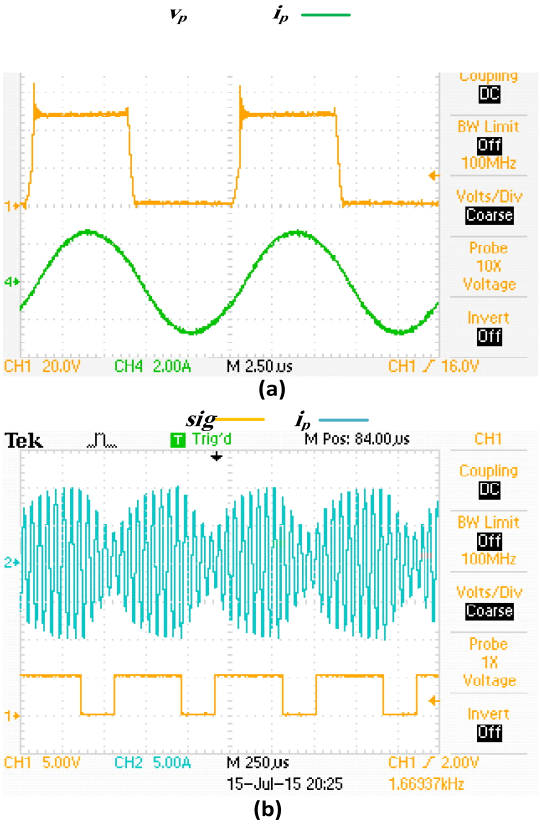

FIGURE 15. (a) V_p and I_p in the experimental test: $\varphi = 15°$ and $k = 0.2$, the maximum power transfer. (b) i_p and control signal in the experimental test.

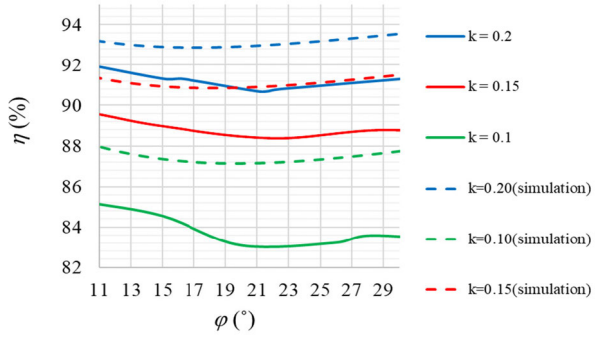

FIGURE 16. The efficiency with respect to φ in different k and SOC = 90%.

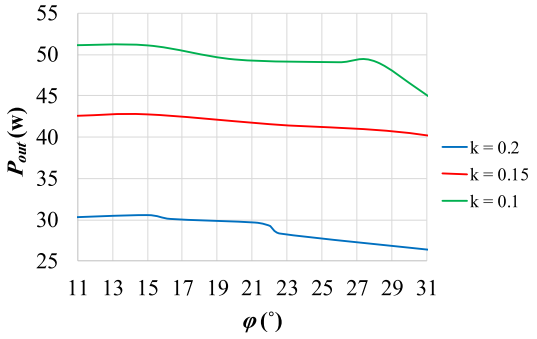

FIGURE 17. Output power with respect to φ in different k and SOC = 90%.

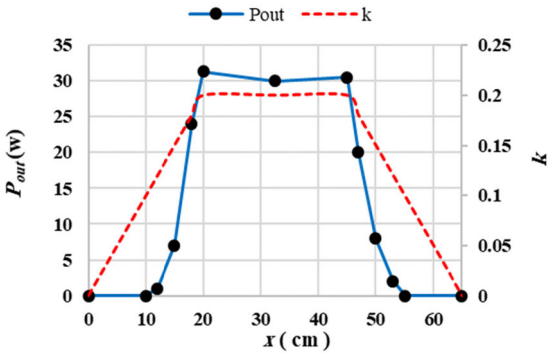

FIGURE 18. Coupling factor and output power with respect to coil displacement.

TABLE 2. Specifications of the laboratory prototype.

PARAMETER	VALUE
C_p	25 nF
C_s	16.8 nF
L_P	159 µH
L_s	236 µH
k_{max}	0.2
r_p	0.3 Ω
r_s	0.7 Ω
The nominal voltage of the battery	28.8 V
V_{DC}	50 V

and the air-gap length of about 5 cm, L_p, L_s, and k_{max} are about 159 μH, 236 μH, and 0.22, respectively. Dimensions of pickup and track coils are shown in Fig. 14. The CT turn ratio is 100 and a 100 Ω resistor is connected to the CT, i.e. 1Amp/Volt gain. The power switches are IRFP260N power MOSFETs driven by IR2104S bootstrap gate drivers. The MCU is ATMEGA16 with an 8-MHz clock pulse. Zero detectors are LT1016 comparators with a propagation delay of about 10 ns. The tunable phase shifter is implemented using two 10 kΩ pots and tuning capacitors of 2.2nF. The fully charged battery pack includes eight 2200mAh 3.6V Li-Ion batteries that are connected in series.

Due to laboratory limitations, DWC is done at a very low speed. Considering the dynamics and settling time of the system, higher speeds lead to a little lower η_e, Fig. 12 (a). Fig. 15 (*a*) shows the maximum power transfer moment that occurs when φ is 15°. In Fig. 15 (*b*), the performance of current control in the experimental test is shown. The current ripple is 6 A. The control signal that turns the inverter on/off is shown in yellow.

Fig. 16 shows the efficiency versus φ in experimental and simulation (dashed lines). Increasing φ leads to a decrease

in efficiency. The maximum efficiency is 91.95% that is obtained in $k = 0.2$ and $\varphi = 11°$.

More reduction in φ and closing to ZVZCS point increases the risk of losing ZVS. Therefore, in experimental tests, φ is kept more than 10°. Fig. 17 represents the output power of the IPT system versus φ in three different values of k. The maximum power is transferred in the range of 14° to 16° that has good adaption with simulation results, Fig. 7.

Fig. 18 (a) represents the coupling factor with respect to coil displacement x. According to coils dimensions, x varies from 0 to 65 cm. Fig. 18 (b) shows P_{out} with respect to x. To avoid damages to coils, I_{sp} is set to 1.05p.u. In this experiment φ is set to 14°.

VII. CONCLUSION

In this paper, TSOS is investigated for DWC of EV. A resonant half-bridge inverter with series-series compensator and UDD coil is used as the charger. The track coil current is employed as the control signal. The aims of this paper are maximum power transfer in acceptable efficiency and ZVS realization. All possible conditions are considered by a sensitivity analysis. An accurate model for equivalent resistance of the load is presented to cover the DWC condition. This model considers the effect of coupling and frequency changes on load resistance, which can make a significant difference in results. As a result, an optimum range is determined for φ as the control variable of the TSOS. In this range, the power transfer is maximum and even in the worst case, the *power deviation* (*PD*) is lower than 2.3%. In this range, the reduction in efficiency in the nominal case is lower than 3.8% compared to the maximum feasible efficiency which is acceptable. Therefore, the maximum power transfer is achieved and the system is robust to phase changes in this range.

To limit the current of the charger in low coupling factor areas, a simple hysteresis control is used. The setpoint of the controller is investigated by the sensitivity analysis to compromise between energy efficiency, transferred energy, and the maximum current of the charger and maximize energy efficiency in the maximum misalignment. The results show the performance and efficiency of the proposed range of phase angle and controller setpoint. The experimental results approved the simulations.

ACKNOWLEDGMENT

The statements made herein are solely the responsibility of the authors.

REFERENCES

[1] A. Namadmalan, B. Jaafari, A. Iqbal, and M. Al-Hitmi, "Design optimization of inductive power transfer systems considering bifurcation and equivalent AC resistance for spiral coils," *IEEE Access*, vol. 8, pp. 141584–141593, 2020.

[2] C. Panchal, S. Stegen, and J. Lu, "Review of static and dynamic wireless electric vehicle charging system," *Eng. Sci. Technol., Int. J.*, vol. 21, no. 5, pp. 922–937, Oct. 2018, doi: 10.1016/j.jestch.2018.06.015.

[3] V. Cirimele, M. Diana, F. Freschi, and M. Mitolo, "Inductive power transfer for automotive applications: State-of-the-art and future trends," *IEEE Trans. Ind. Appl.*, vol. 54, no. 5, pp. 4069–4079, Sep. 2018, doi: 10.1109/TIA.2018.2836098.

[4] D. Patil, M. K. McDonough, J. M. Miller, B. Fahimi, and P. T. Balsara, "Wireless power transfer for vehicular applications: Overview and challenges," *IEEE Trans. Transport. Electrific.*, vol. 4, no. 1, pp. 3–37, Mar. 2018, doi: 10.1109/TTE.2017.2780627.

[5] Z. Zhang, H. Pang, A. Georgiadis, and C. Cecati, "Wireless power transfer—An overview," *IEEE Trans. Ind. Electron.*, vol. 66, no. 2, pp. 1044–1058, Feb. 2019, doi: 10.1109/TIE.2018.2835378.

[6] G. A. Covic and J. T. Boys, "Modern trends in inductive power transfer for transportation applications," *IEEE J. Emerg. Sel. Topics Power Electron.*, vol. 1, no. 1, pp. 28–41, Mar. 2013, doi: 10.1109/JESTPE.2013.2264473.

[7] S. Lukic and Z. Pantic, "Cutting the cord: Static and dynamic inductive wireless charging of electric vehicles," *IEEE Electrific. Mag.*, vol. 1, no. 1, pp. 57–64, Sep. 2013, doi: 10.1109/MELE.2013.2273228.

[8] A. Ahmad, M. S. Alam, and R. Chabaan, "A comprehensive review of wireless charging technologies for electric vehicles," *IEEE Trans. Transport. Electrific.*, vol. 4, no. 1, pp. 38–63, Mar. 2018, doi: 10.1109/TTE.2017.2771619.

[9] M. Pazos-Revilla, A. Alsharif, S. Gunukula, T. N. Guo, M. Mahmoud, and X. Shen, "Secure and privacy-preserving physical-layer-assisted scheme for EV dynamic charging system," *IEEE Trans. Veh. Technol.*, vol. 67, no. 4, pp. 3304–3318, Apr. 2018, doi: 10.1109/TVT.2017.2780179.

[10] Q. Deng, J. Liu, D. Czarkowski, M. Bojarski, J. Chen, W. Hu, and H. Zhou, "Edge position detection of on-line charged vehicles with segmental wireless power supply," *IEEE Trans. Veh. Technol.*, vol. 66, no. 5, pp. 3610–3621, May 2017, doi: 10.1109/TVT.2016.2598183.

[11] Y. Shin, K. Hwang, J. Park, D. Kim, and S. Ahn, "Precise vehicle location detection method using a wireless power transfer (WPT) system," *IEEE Trans. Veh. Technol.*, vol. 68, no. 2, pp. 1167–1177, Feb. 2019, doi: 10.1109/TVT.2018.2885942.

[12] S. Jeong, Y. J. Jang, D. Kum, and M. S. Lee, "Charging automation for electric vehicles: Is a smaller battery good for the wireless charging electric vehicles?" *IEEE Trans. Autom. Sci. Eng.*, vol. 16, no. 1, pp. 486–497, Jan. 2019, doi: 10.1109/TASE.2018.2827954.

[13] S. Y. Jeong, J. H. Park, G. P. Hong, and C. T. Rim, "Autotuning control system by variation of self-inductance for dynamic wireless EV charging with small air gap," *IEEE Trans. Power Electron.*, vol. 34, no. 6, pp. 5165–5174, Jun. 2019, doi: 10.1109/TPEL.2018.2866412.

[14] G. A. Covic and J. T. Boys, "Inductive power transfer," *Proc. IEEE*, vol. 101, no. 6, pp. 1276–1289, Jun. 2013, doi: 10.1109/JPROC.2013.2244536.

[15] N. Liu and T. G. Habetler, "Design of a universal inductive charger for multiple electric vehicle models," *IEEE Trans. Power Electron.*, vol. 30, no. 11, pp. 6378–6390, Nov. 2015, doi: 10.1109/TPEL.2015.2394734.

[16] A. Babaki, S. Vaez-Zadeh, and A. Zakerian, "Performance optimization of dynamic wireless EV charger under varying driving conditions without resonant information," *IEEE Trans. Veh. Technol.*, vol. 68, no. 11, pp. 10429–10438, Nov. 2019, doi: 10.1109/TVT.2019.2944153.

[17] A. Zakerian, S. Vaez-Zadeh, and A. Babaki, "A dynamic WPT system with high efficiency and high power factor for electric vehicles," *IEEE Trans. Power Electron.*, vol. 35, no. 7, pp. 6732–6740, Jul. 2020, doi: 10.1109/TPEL.2019.2957294.

[18] N. Y. Kim, K. Y. Kim, J. Choi, and C.-W. Kim, "Adaptive frequency with power-level tracking system for efficient magnetic resonance wireless power transfer," *Electron. Lett.*, vol. 48, no. 8, pp. 452–454, Apr. 2012, doi: 10.1049/el.2012.0580.

[19] U. K. Madawala, M. Neath, and D. J. Thrimawithana, "A power–frequency controller for bidirectional inductive power transfer systems," *IEEE Trans. Ind. Electron.*, vol. 60, no. 1, pp. 310–317, Jan. 2013, doi: 10.1109/TIE.2011.2174537.

[20] A. Namadmalan and J. S. Moghani, "Tunable self-oscillating switching technique for current source induction heating systems," *IEEE Trans. Ind. Electron.*, vol. 61, no. 5, pp. 2556–2563, May 2014, doi: 10.1109/TIE.2013.2272278.

[21] A. Moosavi, S. S. Mortazavi, and A. Namadmalan, "Analysis of dynamic wireless charging using tunable self-oscillating method," *Int. J. Electron.*, vol. 106, no. 11, pp. 1746–1768, Nov. 2019, doi: 10.1080/00207217.2019.1616226.

[22] A. Namadmalan, "Self-oscillating tuning loops for series resonant inductive power transfer systems," *IEEE Trans. Power Electron.*, vol. 31, no. 10, pp. 7320–7327, Oct. 2016, doi: 10.1109/TPEL.2015.2508742.

[23] A. Namadmalan, "Self-oscillating pulsewidth modulation for inductive power transfer systems," *IEEE J. Emerg. Sel. Topics Power Electron.*, vol. 8, no. 2, pp. 1813–1820, Jun. 2020, doi: 10.1109/JESTPE.2019.2916425.
[24] K. Aditya and S. S. Williamson, "Design guidelines to avoid bifurcation in a series–series compensated inductive power transfer system," *IEEE Trans. Ind. Electron.*, vol. 66, no. 5, pp. 3973–3982, May 2019, doi: 10.1109/TIE.2018.2851953.
[25] S. Y. Choi, B. W. Gu, S. Y. Jeong, and C. T. Rim, "Advances in wireless power transfer systems for roadway-powered electric vehicles," *IEEE J. Emerg. Sel. Topics Power Electron.*, vol. 3, no. 1, pp. 18–36, Mar. 2015, doi: 10.1109/JESTPE.2014.2343674.
[26] M. Bertoluzzo, G. Buja, and H. K. Dashora, "Design of DWC system track with unequal DD coil set," *IEEE Trans. Transport. Electrific.*, vol. 3, no. 2, pp. 380–391, Jun. 2017, doi: 10.1109/TTE.2016.2646740.
[27] J. M. Jacob, *Industrial Control Electronics: Applications and Design*. Upper Saddle River, NJ, USA: Prentice-Hall, 1988.
[28] T. L. Bartelt, *Industrial Control Electronics*. Clifton Park, NY, USA: Delmar-Cengage Learning, 2012.

S. ABBAS MOOSAVI was born in Izeh, Khuzestan, Iran, on January 4, 1987. He received the B.Sc., M.Sc., and Ph.D. degrees in electrical engineering from the Shahid Chamran University of Ahvaz, Ahvaz, Iran, in 2010, 2013, and 2019, respectively. He is currently an Assistant Professor with the Department of Electrical Engineering, Abadan Branch, Islamic Azad University, Iran. His current research interests include power electronics, inductive power transfer, and renewable energy conversion.

S. SAEIDALLAH MORTAZAVI was born in Behbahan, Iran, on February 8, 1964. He received the B.Sc. and M.Sc. degrees in electrical engineering from Ferdowsi University, Mashad, Iran, in 1989 and 1992, respectively, and the Ph.D. degree in electrical engineering from IIT Delhi, in January 1999. Since 1999, he has been a Professor with the Department of Electrical Engineering, Shahid Chamran University of Ahvaz, Iran. His research interests include intelligent control and power system control and operation.

ALIREZA NAMADMALAN received the B.Sc. degree from the Isfahan University of Technology, Isfahan, Iran, in 2009, and the M.Sc. and Ph.D. degrees (Hons.) in electrical engineering from the Amirkabir University of Technology, Tehran, Iran, in 2011 and 2014, respectively. From 2012 to 2014, he had research activities with the Research and Development Center, Damavand Induction Furnace Company, Damavand, Iran, where he was working on industrial induction heating systems. He is currently an Assistant Professor with the Department of Electrical and Computer Engineering, Jundi-Shapur University of Technology, Dezful, Iran. His current research interests include power electronics, electromagnetic design using finite element methods, inductive power transfer, and renewable energy conversion.

ATIF IQBAL (Senior Member, IEEE) received the B.Sc. (Hons.) and M.Sc. (engineering) degrees in power system and drives from Aligarh Muslim University (AMU), Aligarh, India, in 1991 and 1996, respectively, the Ph.D. degree from Liverpool John Moores University, Liverpool, U.K. in 2006, and the D.Sc. (Habilitation) degree from the Gdansk University of Technology, Poland, in 2019. He is currently a Full Professor of Electrical Engineering with Qatar University, Doha, Qatar, and a Former Full Professor of Electrical Engineering with AMU. He has been a Lecturer with the Department of Electrical Engineering, AMU, since 1991, where he has served as a Full Professor, till August 2016. He has published widely in international journals and conferences. He has authored/coauthored more than 380 research articles and two books and three chapters in two other books. He has supervised several large Research and Development projects. His research findings related to power electronics and renewable energy sources. His research interests include modeling and simulation of power electronic converters, control of multiphase motor drives, and renewable energy sources. He is also a Fellow of IET, U.K., and IE, India. He was a recipient of the Outstanding Faculty Merit Award AY, from 2014 to 2015, the Research Excellence Award from Qatar University, the Maulana Tufail Ahmad Gold Medal for standing first at B.Sc. Engg. Exams from AMU, in 1991, and best research papers awards from IEEE ICIT-2013, IET SEISCON-2013, SIGMA 2018, IEEE ICIOT 2020, and ICRP 2020. He is also an Associate Editor of the IEEE TRANSACTIONS ON INDUSTRIAL ELECTRONICS and IEEE ACCESS and the Editor-in-Chief of the *Journal of Electrical Engineering* (i-manager).

MOHAMMED AL-HITMI (Member, IEEE) was born in Qatar, in 1968. He received the B.Sc. degree in electrical engineering from Qatar University, Doha, Qatar, in 1992, and the M.S. and Ph.D. degrees in control engineering from The University of Sheffield, in 1994 and 2002, respectively. He is currently an Associate Professor of Electrical Engineering with Qatar University. His research interests include control systems theory, neural networks, fuzzy control, and electric drive systems.